JPE 19-1-15

https://doi.org/10.6113/JPE.2019.19.1.158
ISSN(Print): 1598-2092 / ISSN(Online): 2093-4718

Comparative Study of Flux Regulation Methods for Hybrid Permanent Magnet Axial Field Flux-switching Memory Machines

Gongde Yang*, Xinghe Fu*, Mingyao Lin*, Nian Li*, and Hao Li†

*School of Electric Engineering, Southeast University, Nanjing, China
†School of Automation, Southeast University, Nanjing, China

Abstract

This research comparatively studies three kinds of flux regulation methods, namely, stored capacitor discharge pulse (SCDP), constant current source pulse (CCSP), and quantitative flux regulation pulse (QFRP), which are used for hybrid permanent magnet (PM) axial field flux-switching memory machines (HPM-AFFSMMs). Through an analysis of the operation principle and the series hybrid PM flux regulation mechanism of the objective machine, the circuit topologies and flux regulation process of these flux regulation methods are addressed in detail. On the basis of a simulation, the flux regulation characteristics of the researched machine during the magnetization and demagnetization processes are comparatively evaluated. Then, machine performance, including back EMF, direct and quadrature axis inductances, and magnetization and demagnetization characteristics, is quantitatively investigated. Results show that the QFRP enables the HPM-AFFSMM to achieve a less harmonic component of back EMF by approximately 7.28% and 7.97% at the magnetization and demagnetization states, respectively, and a more complete magnetization process than the SCDP and CCSP.

Key words: Constant current source pulse, Flux control, Flux regulation, Memory machine, Quantitative flux regulation pulse, Stored capacitor discharge pulse

NOMENCLATURE

MM	Memory machine
PM	Permanent magnet
MS	Magnetization state
LCF	Low coercive force
SCDP	Stored capacitor discharge pulse
CCSP	Constant current source pulse
QFRP	Quantitative flux regulation pulse
MMF	Magnetomotive force
HPM-AFFSMM	Hybrid PM axial field flux-switching MM

I. INTRODUCTION

Memory machines (MMs), which regulate the air gap flux density by applying a pulse to tune the magnetization state (MS) of low-coercive-force (LCF) permanent magnet (PM) material, are deemed to be true flux-adjustable PM machines [1]. In recent decades, various MMs have been developed. On the basis of PM position, these MMs can be classified into rotor-PM type [2]-[9] and stator-PM type [10]-[21]. For rotor-PM MMs, armature winding is utilized to adjust the MS of the LCF PM, which decreases the system volume and cost. Nevertheless, they suffer from the inevitably undesirable demagnetization caused by the armature reaction, complicated vector control, and difficult thermal dissipation. Considering the demerits of rotor-PM MMs, stator-PM MMs, including doubly salient MMs [10]-[13] and flux-switching MMs [14]-[21], have been exploited. Although the machine configuration of stator-PM MMs is complicated and an extra converter is required for the MS selection of LCF PM, the extra excitation winding simplifies the vector control and the MS regulation. Meanwhile, the PM, armature winding, and magnetization winding are all on the stator, thereby resulting in expedient

Manuscript received Apr. 28, 2018; accepted Oct. 18, 2018
Recommended for publication by Associate Editor Gaolin Wang.
†Corresponding Author: mylin@seu.edu.cn
Tel: +25-83794169-806, Fax: +25-83794169-806, Southeast University
*School of Electric Engineering, Southeast University, China

thermal management. Hence, significant attention has been given to stator-PM MMs.

Given the flux regulation characteristic and the PM leakage flux linkage, precisely obtaining the actual PM flux linkage is difficult. Therefore, the bivariate table between the PM flux linkage and the pulse is employed. That is, when the required PM flux linkage is given, the corresponding pulse should be imposed. Given that the pulse decides whether the stator-PM MMs can achieve a good flux regulation effect or not, the means of generating an accurate pulse is the key issue in PM flux linkage control. At present, several types of flux regulation methods, namely, stored capacitor discharge pulse (SCDP) [14]-[18], constant current source pulse (CCSP) [19], [20], and quantitative flux regulation pulse (QFRP) [21], are studied and applied for tuning the MS of LCF PMs.

Given the advantages of the flux concentration effect, the robust rotor structure, and the stable magnetic performance of the LCF PM, the hybrid PM axial field flux-switching memory machine (HPM-AFFSMM) is utilized as the objective machine to compare the flux regulation characteristics of the three methods. This paper is organized as follows. In Section II, the operating principle and the series hybrid PM flux regulation mechanism of the HPM-AFFSMM are described. Then, the circuit topologies and operating process of the three types of flux regulation methods are presented in Section III. Finally, the simulation and experiment are performed on the researched HPM-AFFSMM to compare the flux regulation performance of the machine quantitatively.

II. Operating Principle and Series Hybrid PM Flux Regulation Mechanism of the HPM-AFFSMM

A. Machine Configuration and Operating Principle

Fig. 1 shows the researched machine configuration, in which the PM materials, including AlNiCo/NdFeB, the armature winding, and the magnetization winding, are all accommodated in the two outer stators. The rotor has neither windings nor PMs, resulting in a robust rotor structure. The two types of PMs are arranged in series in "U"-shaped laminated segments, and the magnetization direction is reversed in polarity from one magnet to the next. The magnetization windings stretch across each "U"-shaped laminated segment.

The operating principle of the machine can be understood from the following two points. First is the flux-switching behavior between stator and rotor poles, that is, the periodical rotor position results in an alternately varying PM flux line, as shown in Fig. 2, where the dotted line denotes the PM flux line, and the solid line represents the excitation flux line. Second, the MS is regulated by the imposed pulse. When the pulse is imposed as shown in Fig. 2(a), the direction of the excitation flux line is in accordance with that of the PM flux line. After the pulse disappears, the PMs can be magnetized.

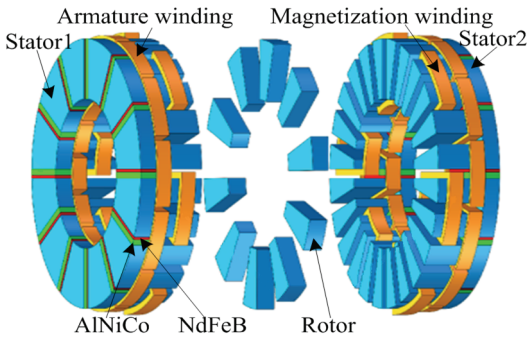

Fig. 1. Machine configuration.

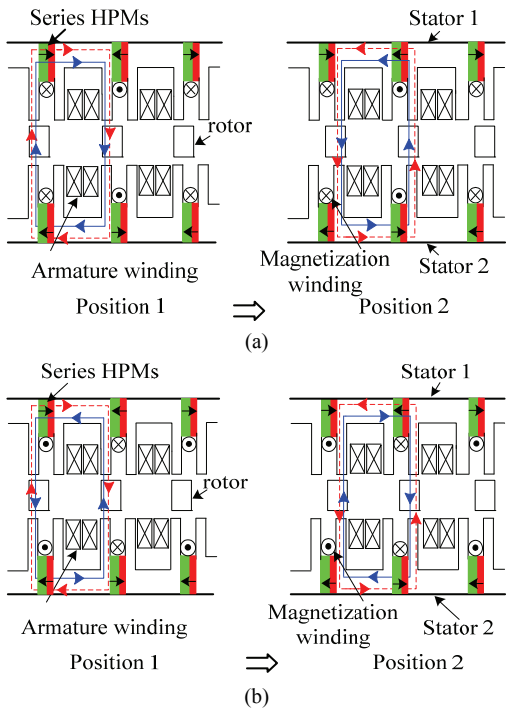

Fig. 2. Operating principle of the researched machine: (a) Magnetization process; (b) Demagnetization process.

By contrast, when the pulse is injected as shown in Fig. 2(b), the direction of the excitation flux line becomes opposite to that of the PM flux line. Once the pulse vanishes, the PMs can be demagnetized.

B. Series Hybrid PM Flux Regulation Mechanism

Given the flux regulation characteristic of AlNiCo, the MS of AlNiCo can be easily regulated by applying a pulse. After the pulse is released, the new MS will be memorized automatically. Flux regulation comprises the magnetization and demagnetization processes. The concrete series hybrid PM flux regulation mechanism, as shown in Fig. 3, is illustrated visually from the magnetization curves of AlNiCo and NdFeB. With the demagnetization process as an example, AlNiCo and NdFeB are first fully magnetized, and their initial working points are assumed to be respectively located at a and A when only the two types of PMs are adopted.

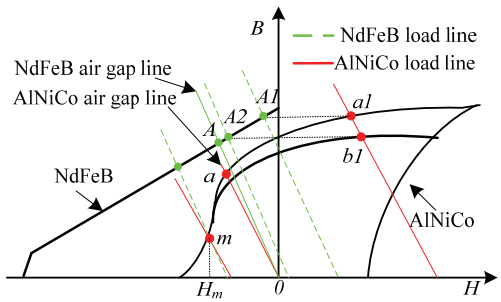

Fig. 3. Illustration of series hybrid PM flux regulation mechanism.

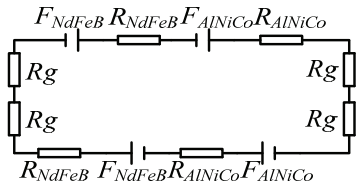

Fig. 4. Equivalent magnetic circuit of the HPM-AFFSMM.

AlNiCo and NdFeB are connected in series, as shown in Fig. 1, and the equivalent magnetic circuit of the machine is shown in Fig. 4. According to Ampere's loop law and Kirchhoff's magnetic circuit law, the relationship between flux density B_{AlNiCo} (B_{NdFeB}) and magnetic field strength H_{AlNiCo} (H_{NdFeB}) is deduced as

$$\begin{cases} B_{AlNiCo} = \dfrac{-\mu_0 A_\delta h_{AlNiCo} H_{AlNiCo} - \mu_0 A_\delta h_{NdFeB} H_{NdFeB}}{2 A_{AlNiCo} \delta} \\ B_{NdFeB} = \dfrac{-\mu_0 A_\delta h_{AlNiCo} H_{AlNiCo} - \mu_0 A_\delta h_{NdFeB} H_{NdFeB}}{2 A_{NdFeB} \delta} \end{cases}, \quad (1)$$

where h_{AlNiCo} (h_{NdFeB}) and A_{AlNiCo} (A_{NdFeB}) respectively represent the AlNiCo (NdFeB) PM thickness, cross section area perpendicular to magnetization direction, δ and A_δ respectively stand for the air-gap length and the cross-sectional area, and μ_0 is the permeability of free space.

Given that AlNiCo and NdFeB are magnetically connected in series and have the same cross-sectional areas perpendicular to the magnetization direction they have the same flux density. On the basis of (1), AlNiCo and NdFeB interact with each other. Consequently, their actual working points will respectively shift from a (A) to a1 ($A1$).

Given the constant magnetomotive force (MMF) generated by NdFeB, the AlNiCo of different MSs must withstand the MMF without the external magnetization field. When external demagnetization MMF of H_m is imposed and then removed, the working point of AlNiCo will track along *a1-a-m-b-b1* and then become immobilized at *b1*. Meanwhile, the working point of NdFeB will be terminated at point *A2* along *A1-A2*. In the same manner, the working points of AlNiCo will vary in other recoil lines on the basis of the corresponding external demagnetization MMF. Similarly, the variation of working points for AlNiCo and NdFeB in the magnetization process can be analyzed when external magnetization MMF is applied.

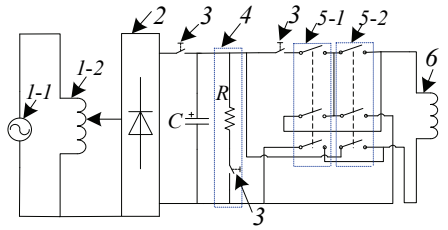

1-1 AC voltage source, 1-2 transformer, 2-rectifier, 3-switch, 4-discharge protect circuit, 5-1 and 5-2 polarity-reversible switches, 6-magnetization winding.

Fig. 5. Circuit topology of the SCDP.

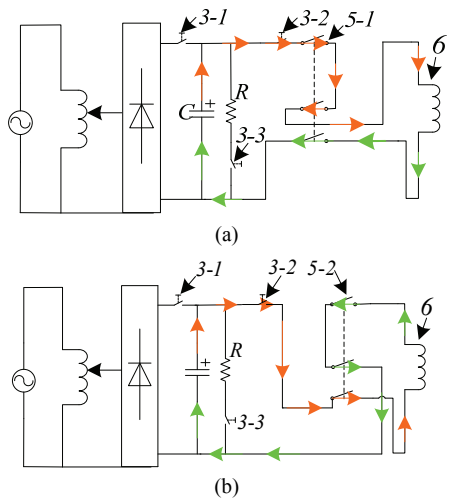

Fig. 6. Bidirectional flux regulation circuit of the SCDP: (a) Magnetization circuit; (b) Demagnetization circuit.

III. Circuit Topologies and Operating Process of Flux Regulation Methods

A. Circuit Topology and Operating Process of the SCDP

Fig. 5 shows the simplified circuit topology of the SCDP, which mainly consists of an AC voltage source, a transformer, a rectifier, several switches, a discharge protect circuit, and polarity-reversible switches. When switch (3-1) is on, as shown in Fig. 6, the AC voltage source charges the stored capacitor through the rectifier. If the voltage of the stored capacitor reaches its required U_a, switch (3-1) will be cut off. To generate the pulse, switch (3-2) turns on. Then, the stored capacitor discharges its energy to the magnetization winding through the polarity-reversible switches. When the magnetization winding parameters listed in Table II are employed, the second-order circuits have an overdamped solution. The pulse first reaches its peak value (i_a). Then, it decays and approaches zero over time. The relationship between U_a and i_a is expressed as

$$i_a = U_a \sqrt{\frac{C}{L_m}} \left(\sqrt{\frac{R_m^2 C}{4L_m}} + \sqrt{\frac{R_m^2 C}{4L_m} - 1} \right)^{-\sqrt{\frac{RC}{4L}} \Big/ \sqrt{\frac{RC}{4L} - 1}}, \quad (2)$$

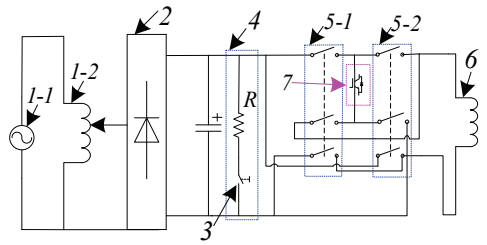

1-1 AC voltage source, 1-2 transformer, 2-rectifier, 3-switch, 4-discharge protect circuit, 5-1 and 5-2 polarity reversible switches, 6-magnetizing winding, 7-power switch.

Fig. 7. Circuit topology of the *CCSP*.

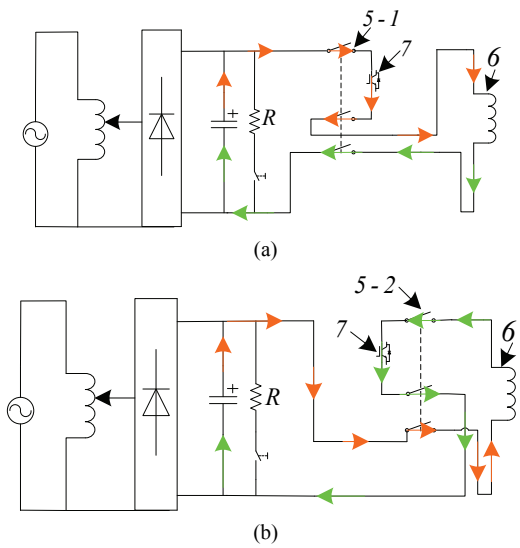

Fig. 8. Bidirectional flux regulation circuit of the *CCSP*: (a) Magnetization circuit; (b) Demagnetization circuit.

where C is the stored capacitor, and R_m and L_m are the resistor and inductor, respectively, of the magnetization winding.

Given that one end of the magnetization winding connects to the ground, switching the excitation field by adjustment of the winding connection type is difficult. Therefore, double polarity-reversible switches are used to change the polarity of the power supply. When AlNiCo must be magnetized, as shown in Fig. 6(a), polarity reversible switch (5-1) is on and (5-2) is off. Otherwise, as shown in Fig. 6(b), polarity-reversible switch (5-2) is on and (5-1) is off. When the system breaks down, the discharge resistor (R) is employed to avoid the harm from the high voltage stored in the capacitor. Switch (3-3) is off during normal operation and on in the case of faults.

B. Circuit Topology and Operating Process of the CCSP

The circuit topology and the bidirectional flux regulation process of the CCSP are shown in Figs. 7 and 8, respectively, and are similar to those of the SCDP. The relationship between U_a and i_a is expressed as

$$i_a = U_a / R_m . \tag{3}$$

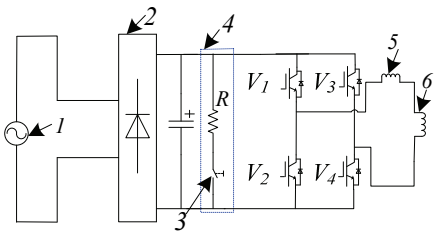

1-AC voltage source, 2-rectifier, 3-switch, 4-discharge protect circuit, 5-filter inductance, 6-magnetization winding.

Fig. 9. Circuit topology of the *QFRP*.

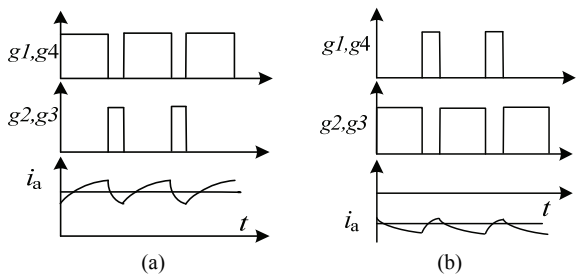

Fig. 10. Bidirectional flux regulation principle of the *QFRP*: (a) Magnetization principle; (b) Demagnetization principle.

Compared with the *SCDP*, the *CCSP* can achieve a flat pulse due to the continuous power supply. However, the distinct differences between the *CCSP* and the *SCDP* are summarized as follows:

1) The stored capacitor must be connected to the rectifier all the time;

2) The power switch is used to regulate the pulse duration.

C. Circuit Topology and Operating Process of the QFRP

The circuit topology of the QFRP is shown in Fig. 9 where V1, V2, V3, and V4 are the four power switches. Unlike methods that use two polarity reversible switches, the QFRP can automatically achieve the direction control of the pulse. When the duty cycle of V1 and V4 is larger than that of V2 and V3, the positive pulse flows through the magnetization winding, as shown in Fig. 10(a). Conversely, the negative pulse traverses the magnetization winding, as shown in Fig. 10(b) where g1, g2, g3, and g4 are the switch signals. The required pulse amplitude can be achieved through the single current closed-loop control. When the control system falls into steady state, the current pulse can be determined as follows:

$$i_a = (2D-1)\frac{U_a}{R_m}, \tag{4}$$

where D is the duty cycle.

IV. Comparison of Flux Regulation Methods

A. Comparison of Flux Regulation Pulse

Under the same magnetization winding parameter, the pulses for the three types of flux regulation methods are qualitatively

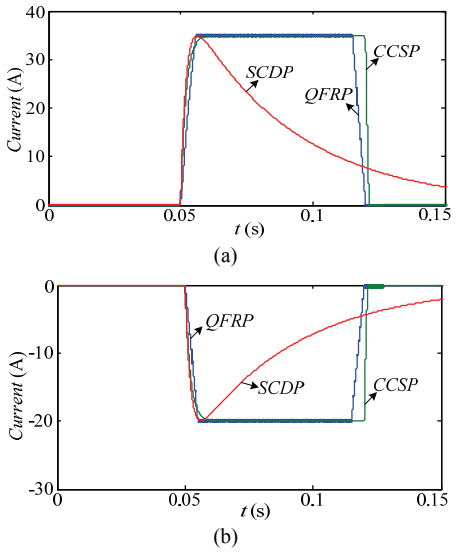

Fig. 11. Pulses of different flux regulation methods under constant parameters: (a) Magnetization pulses; (b) Demagnetization pulses.

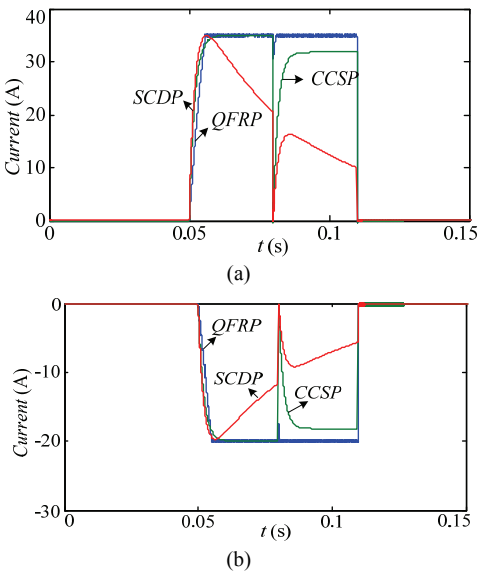

Fig. 12. Pulses of different flux regulation methods under varied parameters: (a) Magnetization pulses; (b) Demagnetization pulses.

compared via Simulink. Under constant magnetization winding parameters, the positive pulses of 35 (A) and the negative pulses of 20 (A) are depicted in Figs. 11(a) and 11(b), respectively, when the flux regulation methods are employed. The SCDP reaches the pulse peak only once. Its pulse width and rising and falling edge cannot be controlled. By contrast, the CCSP can control its pulse width but cannot regulate the rising and falling edge. Meanwhile, the QFRP realizes quantitative and bidirectional control without any manual adjustment of the input DC voltage and use of any polarity-reversible switch.

The positive and negative pulses of the three flux regulation methods that correspond to Figs. 11(a) and 11(b) with a sudden rise in magnetization winding resistor of approximately 10% are shown in Figs. 12(a) and 12(b). QFRP is insensitive to the magnetization winding resistor variation, unlike the two other methods.

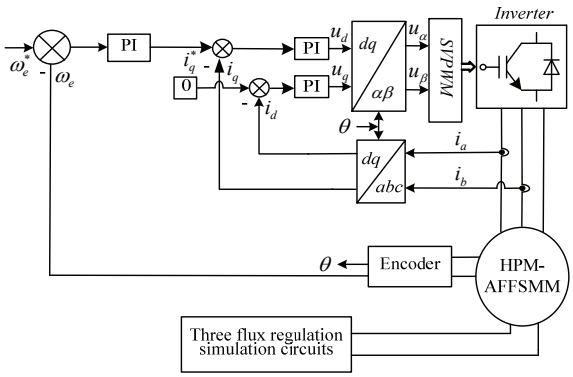

Fig. 13. Control block diagram of researched machine with three kinds of flux regulation methods.

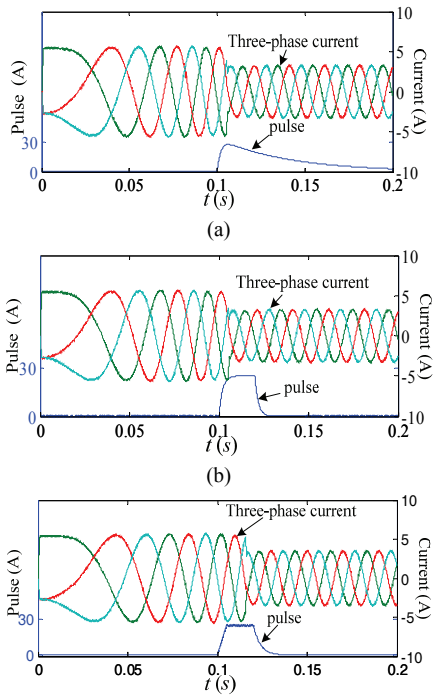

Fig. 14. Simulated magnetization pulses and three-phase current: (a) *SCDP*; (b) *CCSP*; (c) *QFRP*.

B. Flux Regulation Performance Comparison of Machine

To verify the flux regulation characteristic of the three flux regulation methods, a control block diagram of the researched machine, which mainly consists of the magnetization winding controller and the armature winding controller, is shown in Fig. 13. Given the flux regulation characteristic of the LCF PM, the PM flux linkage of the machine is employed as an input variable. The three kinds of flux regulation methods function as the magnetization controller for generating pulse. The armature winding controller, which utilizes the traditional outer speed loop and inner current loop structure, is adopted

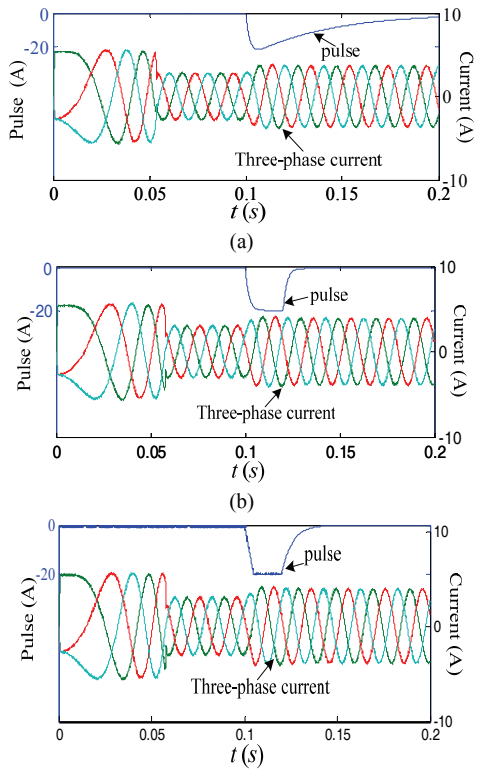

Fig. 15. Simulated demagnetization pulses and three-phase current: (a) *SCDP*; (b) *CCSP*; (c) *QFRP*.

TABLE I
HARMONIC COMPONENT RATIOS OF THE PHASE-A CURRENT

Method	Magnetization process	Demagnetization process
SCDP	1.78%	1.59%
CCSP	1.73%	1.47%
QFRP	1.72%	1.25%

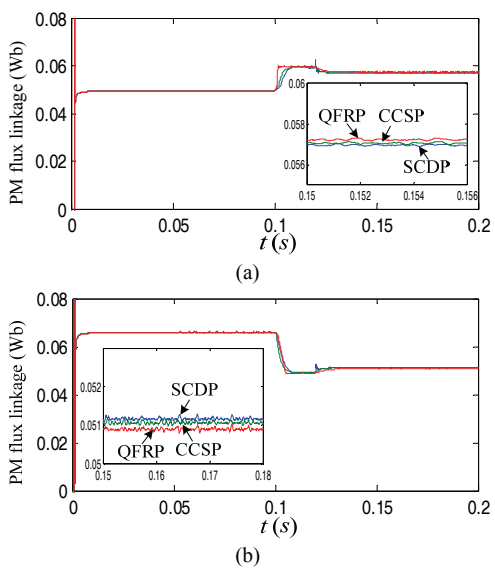

Fig. 16. PM flux linkages of different flux regulation methods: (a) Magnetization process; (b) Demagnetization process.

to produce the firing signal of each power switch in the armature inverter.

The pulses and the three-phase current of the machine at the speed of 300 r/min with a load of 2.8 N·m and with use of SCDP, CCSP, and QFRP are shown as Figs. 14 and 15. During the magnetization process, as shown in Fig. 14, a pulse of 25 A is applied when the initial PM flux is set to 0.05 Wb. During the demagnetization process shown in Fig. 15, a pulse of 20 A is imposed when the initial PM flux is set to 0.0667 Wb.

The harmonic component ratios of phase-A current corresponding to the magnetization and demagnetization processes of SCDP, CCSP, and QFRP with the machine in steady state are listed in Table I. *QFRP* has a better flux regulation effect than does *SCDP* and *CCSP*. Furthermore, we can confirm under the same load torque that the greater the PM flux linkage, the less the armature current.

The PM flux of the machine during magnetization and demagnetization is shown in Fig. 16, which corresponds to Figs. 14 and 15. The machine with QFRP exhibits a larger PM flux during the magnetization process and obtains a better demagnetization effect during the demagnetization process than do the other methods.

V. EXPERIMENTAL VERIFICATION

To compare the flux regulation characteristics of the three flux regulation methods further, the test platform shown in Fig. 17 is used for experimental verification. The researched 12/10-pole HPM-AFFSMM, which are mechanically coupled with a DC dynamometer via a dynamic torque transducer, is adopted as an objective machine for the flux regulation process, and a TSL 160 turntable is employed to measure the machine inductance, including the *dq*-axis inductances. The corresponding parameters of the HPM-AFFSMM related to the flux regulation methods are listed in Table II. The designed circuits of the three kinds of flux regulation methods are shown in Fig. 19; Fig. 19(a) is used for *SCDP*, and Fig. 19(b) can be used for either *CCSP* or *QFRP*. The designed circuit parameters related to the flux regulation methods are listed in Table III.

A. Back EMF

The pulses and the three-phase back EMF of the HPM-AFFSMM at the speed of 180 r/min with no load and with use of SCDP, CCSP, and QFRP are shown in Figs. 19 and 20. During the magnetization process, as shown in Fig. 19, a positive pulse of 30 A is applied after the PMs are fully demagnetized. The RMS values of the phase-A back EMF are 6.25, 6.32, and 6.4 V for SCDP, CCSP, and QFRP, respectively.

Similarly, during the demagnetization process shown in Fig. 20, a negative pulse of 30 A is applied after the PMs are fully magnetized. The RMS values of the phase-A back EMF

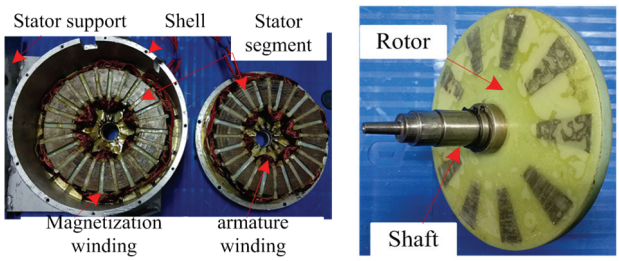

(a)

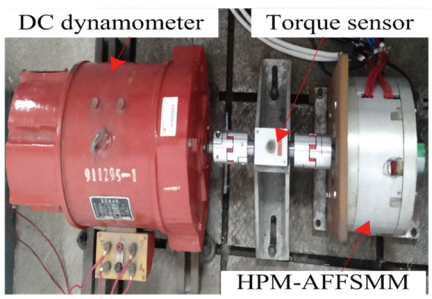

(b)

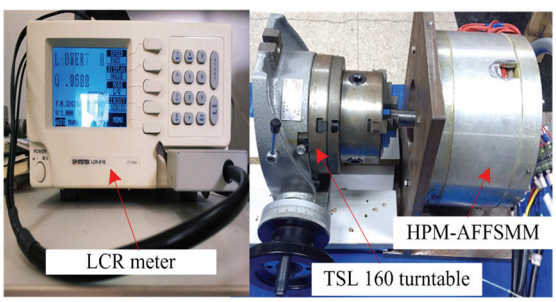

(c)

Fig. 17. Prototype and test platform: (a) Stator; (b) Rotor; (c) Back EMF measurement; (d) Inductance measurement.

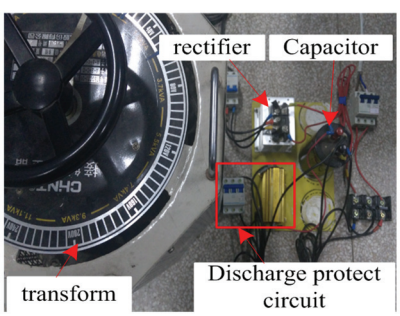

(a)

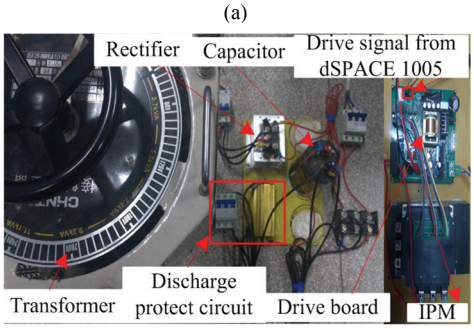

(b)

Fig. 18. Designed circuits of the three flux regulation methods: (a) *SCDP*; (b) *CCSP* and *QFRP*.

TABLE II
DESIGNED MACHINE PARAMETERS RELATED TO THE FLUX REGULATION METHODS

Parameter	Value	Unit
Magnetization winding resistance R_m	4.3	Ω
Magnetization winding inductance L_m	0.0083	H
AlNiCo magnetization thickness	2	*mm*
AlNiCo length	39	*mm*
AlNiCo width	15	*mm*
NdFeB magnetization thickness	4	*mm*
NdFeB length	39	*mm*
NdFeB width	15	*mm*

TABLE III
DESIGNED CIRCUIT PARAMETERS RELATED TO THE FLUX REGULATION METHODS

Parameter	Value	Unit
Rectified input voltage V_{ac}	220	V
Stored capacitor C	10000	uF
Filter inductance L	0.008	H
Discharge circuit resistance R	110	Ω
Proportional coefficient k_p	1.2	-
Integral coefficient	4.3	-

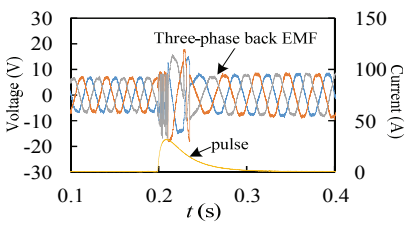

(a)

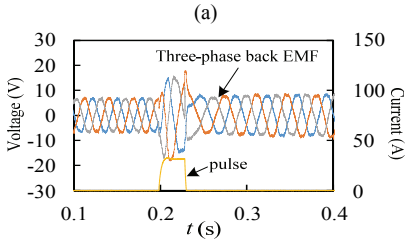

(b)

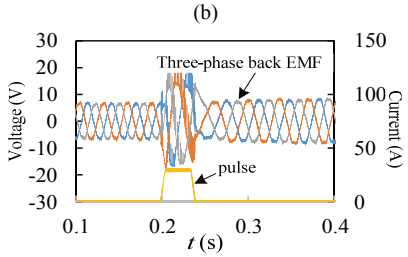

(c)

Fig. 19. Measured magnetization pulses and three-phase back EMF: (a) *SCDP*; (b) *CCSP*; (c) *QFRP*.

are 6.28, 6.35, and 6.43 V, respectively. These findings reveal that QFRP enables the machine to obtain a larger back-EMF than do the two other methods.

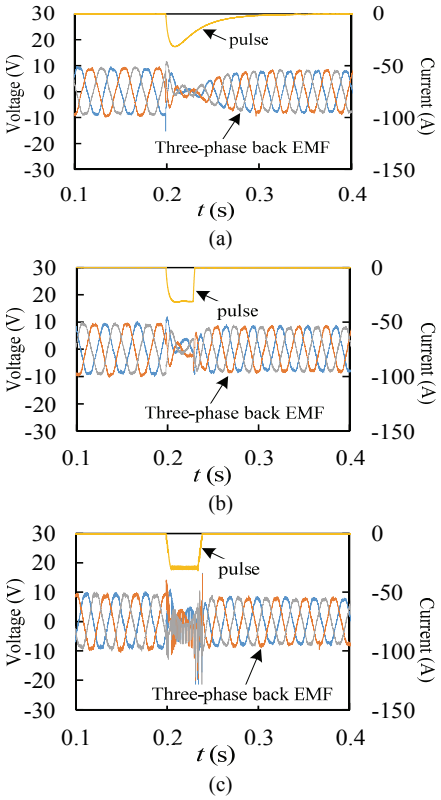

Fig. 20. Measured demagnetization pulses and three-phase back EMF: (a) *SCDP*; (b) *CCSP*; (c) *QFRP*.

TABLE IV
HARMONIC COMPONENT RATIOS OF THE PHASE-A BACK EMF

Method	Magnetization process	Demagnetization process
SCDP	8.42%	8.39%
CCSP	7.76%	7.15%
QFRP	7.28%	7.97%

The harmonic component ratios of the phase-A back EMF, corresponding to Figs. 19 and 20, after the disappearance of the pulse, are listed in Table IV. QFRP enables the machine to have fewer back EMF harmonic components than do SCDP and CCSP.

B. Inductance Characteristic

As shown in Figs. 19 and 20, the three-phase back EMFs of the machine are sinusoidal and thus suitable for the BLAC operation. Thus, direct axis inductance (Ld) and quadrature axis inductance (Lq) are the important parameters for vector control. The direct and quadrature axis inductances of the machine for different MSs under rated current are shown in Figs. 21 and 22, respectively. For each MS of different flux regulation methods, the direct and quadrature axis inductances are quite close, which shows the small saliency ratio of the machine. Furthermore, the direct or quadrature axis inductances of the full MS are less than those of the other MSs due to the slight magnetic saturation in the iron core. Meanwhile, the direct or quadrature axis inductances

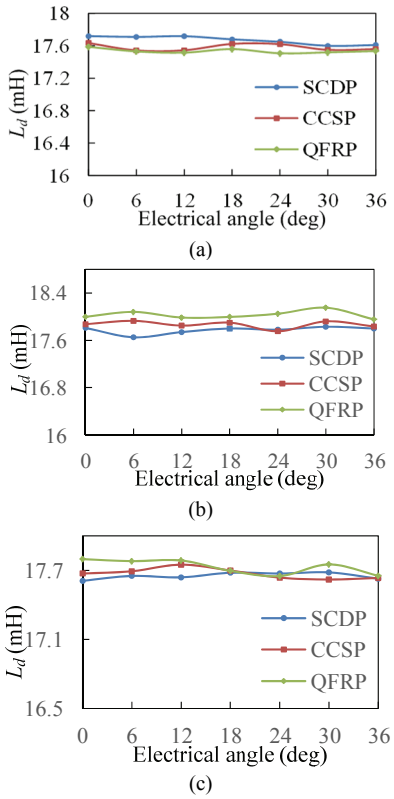

Fig. 21. Measured direct inductances of HPM-AFFSMM: (a) Full MS; (b) Half MS; (c) Full demagnetization state.

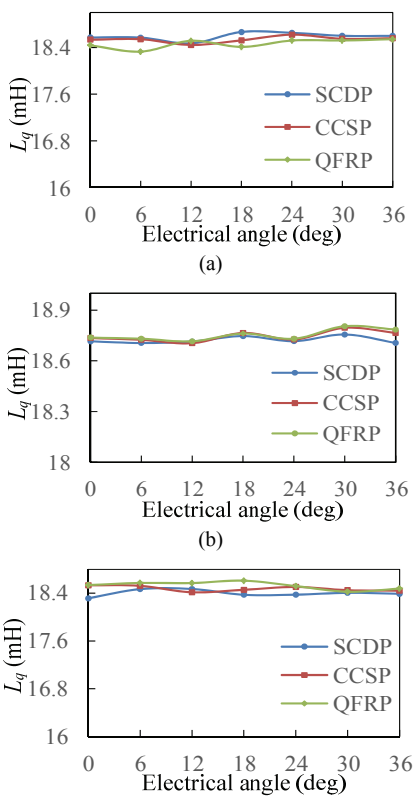

Fig. 22. Measured quadrature inductances of HPM-AFFSMM: (a) Full MS; (b) Half MS; (c) Full demagnetization state.

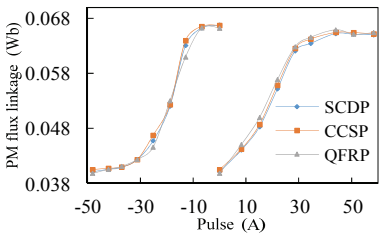

Fig. 23. Flux regulation characteristic curves.

with QFRP are smaller than those with SCDP and CCSP under full MS. Otherwise, they are quite larger under the two other MSs.

C. Magnetization and Demagnetization Characteristic

The relationship between the PM flux linkage and the pulses is determined and shown in Fig. 23. Owing to the magnetic saturation of the iron core caused by the large pulse during the magnetization process, the magnetization process is relatively more difficult than the demagnetization process. Besides, when the measurement tolerance is ignored, the machine with QFRP has a more complete demagnetization process and a worse nonlinear magnetization process than those with SCDP and CCSP.

VI. Conclusions

In this work, several types of flux regulation methods, namely, SCDP, CCSP, and QFRP, are studied and applied to tune the MS of the LCF PM in stator-PM MMs. From the perspectives of circuit topologies and flux regulation processes, the construction and operation of the SCDP and the CCSP are simple, and their maintenance is convenient. However, a pulse of a certain amplitude and direction is not easily generated because it is affected by the manual adjustment of the DC voltage and the winding parameter. Nevertheless, QFRP achieves the quantitative and bidirectional control of pulse without manual adjustment of the input DC voltage and use of a polarity-reversible switch. Furthermore, QFRP is insensitive to the machine parameter. During the magnetization and demagnetization, the flux regulation performance of the researched machine, including the back EMF, *dq*-axis inductance, and the magnetization and demagnetization characteristics, show that the QFRP enables the stator-PM MMs to achieve a better flux regulation effect than do the two other methods. Therefore, QFRP is suitable for the online PM flux linkage control of the stator-PM MM. In future work, the flux density of the PM surface and the cogging torque with the three flux regulation methods will be investigated for an analysis of flux regulation performance.

Acknowledgment

The authors gratefully acknowledge the National Natural Science Foundation of China (Project Nos. 6516000034, 51277025, 51577027) and the Natural Science Foundation of Jiangsu Province (Project BK20161425). The authors also thank the China Scholarship Council for their support for a one-year joint Ph.D. student study to Nottingham University for Gongde Yang (Project No. 201806090269).

References

[1] V. Ostovic, "Memory motors," *IEEE Ind. Appl. Mag.*, Vol. 9, No. 1, pp. 52-61, Jan. 2003.

[2] H. Liu, H. Lin, S. Fang, and Z. Q. Zhu, "Permanent magnet demagnetizing physics of a variable flux memory motor," *IEEE Trans. Magn.*, Vol. 45, No. 10, pp. 4736-4739, Oct. 2009.

[3] H. Liu, H. Lin, Z. Q. Zhu, M. Huang, and P. Jin, "Permanent magnet remagnetizing physics of a variable flux memory motor," *IEEE Trans. Magn.*, Vol. 46, No. 6, pp. 1679-1682, Jun. 2010.

[4] M. Ibrahim, L. Masisi, and P. Pillay, "Design of variable flux PM machine for reduced inverter rating," *IEEE Trans. Ind. Appl.*, Vol. 51, No. 5, pp. 3666-3674, Sep. 2014.

[5] T. Fukushige, N. Limsuwan, T. Kato, K. Akatsu, and R. D. Lorenz, "Efficiency contours and loss minimization over a driving cycle of a variable flux flux-intensifying interior machine," *IEEE Trans. Ind. Appl.*, Vol. 51, No. 4, pp. 2984-2989, Jul. 2015.

[6] S. Maekawa, K. Yuki, M. Matsushita, I. Nitta, Y. Hasegawa, and T. Shiga, "Study of the magnetization method suitable for fractional slot concentrated-winding variable magnetomotive force memory motor," *IEEE Trans. Power Electron.*, Vol. 29, No. 9, pp. 4877-4887, Sep. 2014.

[7] D. Wu, Z. Q. Zhu, X. Liu, A. Pride, R. P. Deodhar, and T. Sasaki, "Cross coupling effect in hybrid magnet memory motor," in *Proc. 7th IET Int. Conf. Power Electron. Mach. Drives*, pp. 1-6, Apr. 2014.

[8] Y. Zhou, Y. Chen, and J. X. Shen, "Analysis and improvement of a hybrid permanent magnet memory motor," *IEEE Trans. Energy Convers.*, Vol. 31, No. 3, pp. 915-923, Sep. 2016.

[9] H. Hua, Z. Q. Zhu, A. Pride, R. P. Deodhar, and T. Sasaki, "A novel variable flux memory machine with series hybrid magnets," *IEEE Trans. Ind. Appl.*, Vol. 53, No. 5, pp. 4396-4405, Sep. 2017.

[10] W. Li, K. T. Chau, Y. Gong, J. Z. Jiang, and F. Li, "A new flux-mnemonic dual-magnet brushless machine," *IEEE Trans. Magn.*, Vol. 47, No. 10, pp. 4223-4226, Oct. 2011.

[11] C. Yu and K. T. Chau, "Design, analysis, and control of dc-excited memory motors," *IEEE Trans. Energy Convers.*, Vol. 26, No. 2, pp. 479-489, Jun. 2011.

[12] X. Zhu, L. Quan, D. Chen, M. Cheng, W. Hua, and X. Sun, "Electromagnetic performance analysis of a new stator-permanent magnet doubly salient flux memory motor using a piecewise-linear hysteresis model," *IEEE Trans. Magn.*, Vol. 47, No. 5, pp. 1106-1109, May. 2011.

[13] X. Zhu, Z. Xiang, L. Quan, W. Wu, and Y. Du, "Multi-mode optimization design methodology for a flux-controllable stator permanent magnet memory motor considering driving cycles," *IEEE Trans. Ind. Appl.*, Vol. 65, No. 7, pp. 5353-5366, Jul. 2018.

[14] H. Yang, H. Lin, S. Fang, Z. Q. Zhu, and Y. Huang, "Flux-regulatable characteristics analysis of a novel switched-flux surface-mounted PM memory machine," *IEEE Trans. Magn.*, Vol. 50, No. 11, Nov. 2014, Art. No. 8103904.
[15] H. Yang, Z. Q. Zhu, H. Lin, S. Fang, and Y. Huang, "Comparative study of novel variable-flux memory machines having stator permanent magnet topologies," *IEEE Trans. Magn.*, Vol. 51, No. 11, Art. No. 8114104, Nov. 2015.
[16] H. Yang, Z. Q. Zhu, H. Lin, S. Fang, and Y. Huang, "Design synthesis of switched flux hybrid permanent magnet memory machines," *IEEE Trans. Energy Convers.,* Vol. 32, No. 1, pp. 65-79, Mar. 2017.
[17] H. Yang, Z. Q. Zhu, H. Lin, S. Fang, and Y. Huang, "Hybrid-excited switched-flux hybrid magnet memory machines," *IEEE Trans. Magn.*, Vol. 52, No. 6, Art. No. 8202215, Jun. 2016.
[18] H. Yang, Z. Q. Zhu, H. Lin, S. Fang, and Y. Huang, "Novel dual stator switched flux memory machines with hybrid magnets," *IEEE Trans. Ind. Appl.*, Vol. 54, No. 3, pp. 2129-2140, May/Jun. 2018.
[19] H. Yang, H. Lin, Z. Q. Zhu, S. Fang, and Y. Huang, "A variable-flux hybrid-PM switched-flux memory machine for EV/HEV applications," *IEEE Trans. Ind. Appl.*, Vol. 52, No. 3, pp. 2203-2214, Aug. 2016.
[20] D. Wu, X. Liu, Z. Q. Zhu, A. Pride, R. Deodhar, and T. Sasaki, "Switched flux hybrid magnet memory machine," *IET Elect. Power Appl.*, Vol. 9, No. 2, pp. 160-170, Feb. 2015.
[21] G. Yang, M. Lin, N. Li, G. Tan, and B. Zhang, "Comparative study of flux regulation Methods for stator permanent magnet memory machine," in *Proc. Inter. Conf. Elec. Mach. Syst. (ICEMS)*, Aug. 2017.

Gongde Yang (S'16) was born in Zhumadian, China, in 1988. He received his B.Eng. from Pingdingshang University, China, in 2012 and his M.Sc. from Jiangnan University, China, in 2015. He is currently working toward obtaining his Ph.D. at Southeast University, Nanjing, China. His major research interests include the drive and control of permanent magnet machines and special machines.

Xinghe Fu received his B.S. in electric machine and drive from Shenyang University of Technology, Shenyang, China, his M.S. in control theory and control engineering from Northeast University, Shenyang, China, and his Ph.D. in electric machine and electric apparatus from the Harbin institute of Technology, Harbin, China. He is currently Associate Professor at the School of Electrical Engineering, Southeast University, Nanjing, China. His research areas are small and special motors, motor control, and industrial automation.

Mingyao Lin received his B.Eng., M.Sc., and Ph.D. in electrical engineering from Southeast University, Nanjing, China, in 1982, 1985, and 1995, respectively. Since 1985, he has been with Southeast University, where he is Professor of electrical engineering. He has authored 160 technical papers and more than 60 patents. His research interests include the design, analysis, and control of permanent magnet machines, wind and photovoltaic power generation technology, and power electronic technology and its industrial applications.

Nian Li was born in Shangqiu, China, in 1989. He received his B.Sc. in electrical engineering and automation from Nanjing University of Science & Technology, Nanjing, China, in 2012. He is working toward obtaining his Ph.D. at the School of Electrical Engineering, Southeast University, Nanjing, China. His research interests include the numerical and electromagnetic design of electrical machines.

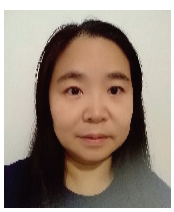

Hao Li received her B.S. in industrial automation from Henan University of Science & Technology, Luoyang, China, her M.S. in control theory and control engineering from Nanjing University of Science and Technology, Nanjing, China, and her Ph.D. in electrical engineering from Southeast University, Nanjing, China. She is a teacher in the School of Automation, Southeast University. Her research interests include the design of permanent magnet machines, and the control and drives of motors.